Underpotential Deposition of Thallium, Lead, and Cadmium at Silver Electrodes Modified with Self-Assembled Monolayers of (3-Mercaptopropyl)trimethoxysilane

Joseph W. F. Robertson,[†] Domenic J. Tiani,[§] and Jeanne E. Pemberton*

Department of Chemistry, University of Arizona, 1306 East University Boulevard, Tucson, Arizona 85721

Received October 26, 2006. In Final Form: November 29, 2006

Investigation of the underpotential deposition (UPD) of three metals—Tl, Pb, and Cd—on Ag surfaces modified with self-assembled monolayers (SAMs) of (3-mercaptopropyl)trimethoxysilane (3MPT) is reported. On the basis of the observation of negative potential shifts for their UPD processes, Tl and Pb undergo UPD directly on the underlying Ag surface by insertion between the Ag−S bond. This process is proposed to occur by penetration of the 3MPT monolayer by hydrated metal ions through spaces in six-membered siloxane rings that form at the terminus of the 3MPT layer after hydrolysis and condensation. In contrast, Cd does not undergo similarly facile UPD at 3MPT-modified Ag electrodes due to a hydrated ion size too large to fit through these openings. The voltammetric evidence that suggests that the hydrated metal cation size, as described by the Stokes diameter, is the primary determinant of Ag electrode accessibility for UPD through the cross-linked 3MPT layer is further supported by molecular mechanics energy minimization computations of six-membered siloxane rings on each of the three low-index faces of Ag. Finally, the 3MPT monolayer is shown to be exceptionally stable to repeated UPD/stripping cycles of Tl and Pb in contrast to SAMs of similar thickness formed from normal alkanethiols.

Introduction

Incorporation of reactive functional groups on the termini of alkanethiol self-assembled monolayers (SAMs) allows covalent bonds to be formed between a SAM and a reactive molecule as a pathway for the effective creation of multilayer structures. Such structures more efficiently restrict access to the underlying metal substrate than normal alkanethiol SAMs. Common reactions employing SAMs have been reviewed recently.[1] Many such reactions are tailored to create brush-like structures that extend away from surfaces,[2−10] while other approaches result in highly cross-linked[11,12] or layered[13−19] polymer networks.

An alternate approach for restricting access to the metal substrate involves monolayers that incorporate self-reactivity for two-dimensional polymerization.[20−34] Such polymerization results in monolayers that retain minimal thickness while providing substrate protection, increased stability, and the incorporation of additional reactive sites onto which covalently tethered multilayer structures can be built.[1,20−41] One such polymerizable SAM is formed with (3-mercaptopropyl)trimethoxysilane (3MPT).[22,23,35−41] This molecule possesses a thiol

* To whom correspondence should be addressed. E-mail: pembertn@u.arizona.edu; voice mail: 520-621-8245; fax: 520-621-8248.

[†] Current address: National Institute for Standards and Technology, Gaithersburg, MD 20899.

[§] Current address: Department of Chemistry, University of North Carolina, Chapel Hill, NC 27599.

(1) Checik, V.; Crooks, R. M.; Stirling, C. J. M. *Adv. Mater.* **2000**, *12*, 1161−1171.
(2) Zhou, B.; Brittain, W. J. *Prog. Polym. Sci.* **2000**, *25*, 677−710.
(3) Zhou, Y.; Bruening, M. L.; Bergbreiter, D. E.; Crooks, R. M.; Wells, M. *J. Am. Chem. Soc.* **1996**, *118*, 3773−3774.
(4) Jordan, R.; Ulman, A. *J. Am. Chem. Soc.* **1998**, *120*, 243−247.
(5) Weck, M.; Jackiw, J. J.; Rossi, R. R.; Weiss, P. S.; Grubbs, R. H. *J. Am. Chem. Soc.* **1999**, *121*, 4088−4089.
(6) Jordan, R.; Ulman, A.; Kang, J. F.; Rafailovich, M. H.; Soolov, J. *J. Am. Chem. Soc.* **1999**, *121*, 1016−1022.
(7) Husemann, M.; Mecerreyes, D.; Hawker, C. J.; Hendrik. J. L.; Shah, R.; Abbott, N. L. *Angew. Chem., Int. Ed.* **1999**, *38*, 647−649.
(8) Jordan, R.; West, N.; Ulman, A.; Nuyken, O. *Macromolecules* **2001**, *34*, 1606−1611.
(9) Schmeler, U.; Jordan, R.; Geyer, W.; Eck, W.; Golzhauser, A.; Grunze, M.; Ulman, A. *Angew. Chem., Int. Ed.* **2003**, *42*, 559−563.
(10) Dyer, D. J.; Feng, J.; Schmidt, R.; Wong, V. N.; Zhao, T.; Yagci, Y. *Macromolecules* **2004**, *37*, 7072−7074.
(11) Prucker, O.; Schimmel, M.; Tovar, G.; Knoll, W.; Ruhe, J. *Adv. Mater.* **1998**, *10*, 1073−1077.
(12) Turyan, I.; Mandler, D. *J. Am. Chem. Soc.* **1998**, *120*, 10733−10742.
(13) Major, J. S.; Blanchard, G. J. *Chem. Mater.* **2002**, *14*, 2567−2573.
(14) Major, J. S.; Blanchard, G. J. *Chem. Mater.* **2002**, *14*, 2574−2581.
(15) Major, J. S.; Blanchard, G. J. *Langmuir* **2002**, *18*, 6548−6553.
(16) Major, J. S.; Blanchard, G. J. *Chem. Mater.* **2002**, *14*, 4320−4327.
(17) Mosley, D. W.; Sellmyer, M. A.; Daida, E. J.; Jacobson, J. M. *J. Am. Chem. Soc.* **2003**, *125*, 10532−10533.
(18) Mendez, S.; Ista, L. K.; Lopez, G. P. *Langmuir* **2003**, *19*, 8115−8116.
(19) Niu, L.; Latonen, R. M.; Kvarnstrom, C.; Ivaska, A. *Electrochim. Acta* **2004**, *49*, 4455−4460.
(20) Kim, T.; Chan, K. C.; Crooks, R. M. *J. Am. Chem. Soc.* **1997**, *119*, 189−193.
(21) Appelhans, D.; Ferse, D.; Adler, H.-J. P.; Plieth, W.; Fikus, A.; Grundke, K.; Schmitt, F. J.; Bayer, T.; Adolphi, B. *Colloids Surf., A* **2000**, *161*, 203−212.
(22) Thompson, W. R.; Cai, M.; Ho, M.; Pemberton, J. E. *Langmuir* **1997**, *13*, 2291−2302.
(23) Thompson, W. R.; Pemberton, J. E. *Chem. Mater.* **1993**, *5*, 241−244.
(24) Yeager, L. J.; Amirsakis, D. G.; Newman, E.; Garrell, R. L. *Tetrahedron Lett.* **1998**, *39*, 8409−8412.
(25) Lukkari, J.; Kleemola, K.; Meretoja, M.; Ollonqvist, T.; Kankare, J. *Langmuir* **1998**, *14*, 1705−1715.
(26) Willicut, R. J.; McCarley, R. J. *J. Am. Chem. Soc.* **1994**, *116*, 10823−10824.
(27) Willicut, R. J.; McCarley, R. J. *Anal. Chim. Acta* **1995**, *307*, 269−276.
(28) Willicut, R. J.; McCarley, R. J. *Adv. Mater.* **1995**, *7*, 759−762.
(29) Mowery, M. D.; Evans, C. E. *Tetrahedron Lett.* **1997**, *38*, 11−14.
(30) Menzel, M.; Horstmann, S.; Mowery, M. D.; Cai, M.; Evans, C. E. *Polymer* **2000**, *41*, 8113−8119.
(31) Duan. L.; Garrett, S. J. *Langmuir* **2001**, *17*, 2986−2994.
(32) Schomburg, K. C.; McCarley, R. L. *Langmuir* **2001**, *17*, 1983−1992.
(33) Cheadle, E. M.; Batchelder, D. N.; Evans, S. D.; Zhang, H. L.; Fukushima, H.; Miyashita, S.; Graupe, M.; Puck, A.; Shmakova, O.; Colorado, R.; Lee, T. R. *Langmuir* **2001**, *17*, 6616−6621.
(34) Chang, Y. H.; Lin, J. T.; Chen, I. W. P.; Chen, C. H. *J. Phys. Chem. B* **2005**, *109*, 19161−19168.
(35) Robertson, J. W.; Cai, M.; Pemberton, J. E. *Adv. Mater.* **2001**, *13*, 662−667.
(36) Kambhampati, D. K.; Jakob, T. A. M.; Robertson, J. W.; Cai, M.; Pemberton, J. E.; Knoll, W. *Langmuir* **2001**, *17*, 1169−1175.
(37) Goss, C. A.; Charych, D. H.; Majda, M. *Anal. Chem.* **1990**, *63*, 85−88.
(38) Zhongdang, X.; Minhua, X.; Jianhua, G.; Dang, H.; Zuhong, L. *Mater. Chem. Phys.* **1998**, *52*, 170−174.
(39) Morneau, A.; Manivannan, A.; Cabrera, C. R. *Langmuir* **1994**, *10*, 3940−3942.
(40) Cai, M.; Ho, M.; Pemberton, J. E. *Langmuir* **2000**, *16*, 3446−3453.
(41) Cai, M.; Pemberton, J. E. *Fresenius' J. Anal. Chem.* **2001**, *369*, 328−334.

10.1021/la063137x CCC: $37.00
Published on Web 03/09/2007

group that covalently binds to metal surfaces and a reactive trimethoxysilane terminal group that participates in hydrolysis and condensation chemistry to form a covalently linked siloxane network.[42] In previous reports from this laboratory, hydrolysis and condensation reactions of 3MPT monolayers at both Ag and Au surfaces were examined,[22,23] and these SAMs were investigated as molecular adhesion layers.[24,25,40,41]

On Ag, Fourier transform infrared reflection−absorption spectroscopy and Raman spectroscopy indicate that 3MPT monolayers initially adopt an orientation in which the S−C bond is largely perpendicular to the surface.[22] However, after hydrolysis and condensation of the trimethoxy terminal groups, the S−C bonds reorient to become more parallel to the surface, and Si−O−Si bonds are formed that are largely parallel to the surface. X-ray photoelectron spectroscopy (XPS) data indicate that only a small percentage (<5%) of the available Si−O bonds are terminated in reactive silanol groups after this process, with the remainder being coupled in siloxane linkages.[22]

Although SAM structures have been analyzed by a host of techniques including FTIR spectroscopy, Raman spectroscopy,[42−44] ellipsometry,[45−50] contact angle measurements,[50−54] XPS,[45,49−51] solution electrochemistry,[50,55−60] and electrochemical impedance spectroscopy,[61−63] the majority of these studies have focused on inert, or nonpolymerizable SAMs with $-CH_3$, −OH, or −COOH terminal groups. These monolayers rely on intermolecular van der Waals interactions for stability, and often cannot withstand certain electrochemical processes that occur at the metal substrate.

Of particular interest for the work reported here are studies on SAMs using metal underpotential deposition (UPD) as a probe.[64−95] In the UPD process, metal ions are reduced at certain foreign metal electrodes at potentials below their reversible reduction potential. This process often occurs for the first one to two monolayers of metal deposited at a potential up to several hundred millivolts below the reversible potential where bulk metal deposits.[96−98] The magnitude of the potential shift from the reversible reduction potential is indicative of the degree of thermodynamic stability that the heterometal affords the first one to two monolayers of electrochemically deposited metal. In voltammetric studies, fine structure in the UPD current−potential response indicates thermodynamic differences in the surface sites on the metal electrode that can be due to a variety of factors, including crystal face (e.g., (110) versus (111) face), the presence of defect sites such as step edges or crystal lattice edges, or the presence of coadsorbates. Given the sensitivity of metal UPD to subtle changes in metal electrode surface chemistry, any small change in this surface chemistry should lead to observable changes in the UPD behavior.

UPD has been used to characterize a number of SAM systems.[64−95] Typical systems studied previously include CH_3-terminated SAMs at Au (111) surfaces using either Ag[65,69,80,82,87] or Cu[64,66−68,74,77,88,94] as the underpotentially deposited metal. In general, the presence of the alkanethiol monolayer kinetically

(42) Brinker, C. J.; Scherer, G. W. *Sol-Gel Science: The Physics and Chemistry of Sol-Gel Processing*; Academic Press: San Diego, CA, 1990.
(43) Bryant, M. A.; Pemberton, J. E. *J. Am. Chem. Soc.* **1991**, *113*, 8284−8293.
(44) Bryant, M. A.; Pemberton, J. E. *J. Am. Chem. Soc.* **1991**, *113*, 3629−3637.
(45) Bryant, M. A.; Joa, S. L.; Pemberton, J. E. *Langmuir* **1992**, *8*, 753−756.
(46) Sheen, C. W.; Shi, J. X.; Martensson, J.; Parikh, A. N.; Allara, D. L. *J. Am. Chem. Soc.* **1992**, *114*, 1514−1515.
(47) Allara, D. L.; Nuzzo, G. R. *Langmuir* **1985**, *1*, 45−52.
(48) Walzak, M. M.; Chung, C.; Stole, S. M.; Widrig, C. A.; Porter, M. D. *J. Am. Chem. Soc.* **1991**, *113*, 2370−2378.
(49) Wasserman, S. R.; Tao, Y. T.; Whitesides, G. M. *Langmuir* **1989**, *5*, 1074−1087.
(50) Bain, C. D.; Troughton, E. B.; Tao, Y. T.; Evall, J.; Whitesides, G. M.; Nuzzo, R. G. *J. Am. Chem. Soc.* **1989**, *111*, 321−335.
(51) Finklea, H. O.; Avery, S.; Lynch, M.; Furtsch, T. *Langmuir* **1987**, *3*, 409−413.
(52) Moskovits, M.; Suh, J. S. *J. Am. Chem. Soc.* **1985**, *107*, 6826−6829.
(53) Laibinis, P. E.; Whitesides, G. W.; Allara, D. L.; Tao, Y. T.; Parikh, Y. T.; Nuzzo, R. G. *J. Am. Chem. Soc.* **1991**, *113*, 7152−7167.
(54) Cohen, S. R.; Naaman, R.; Sagiv, J. *J. Phys. Chem.* **1986**, *90*, 3054−3056.
(55) Whitesides, G. M.; Laibinis, P. E. *Langmuir* **1990**, *6*, 87−96.
(56) Porter, M. D.; Bright, T. B.; Allara, D. L.; Chidsey, C. E. D. *J. Am. Chem. Soc.* **1987**, *109*, 3559−3568.
(57) Finklea, H. O.; Robinson, L. R.; Blackburn, A.; Richter, B.; Allara, D. L. *Langmuir* **1986**, *2*, 239−244.
(58) Nuzzo, R. G.; Dubois, L. H.; Allara, D. L. *J. Am. Chem. Soc.* **1990**, *117*, 558−559.
(59) Wanunu, M.; Vaskevich, A.; Rubinstein, I. *Isr. J. Chem.* **2005**, *45*, 337−344.
(60) Dia, P.; Hou, Q.; Guo, M.; Xiang, M.; Zhang, Q. *J. Electroanal. Chem.* **2006**, *597*, 103−110.
(61) Boubour, E.; Lennox, R. B. *J. Phys. Chem. B* **2000**, *104*, 9004−9010.
(62) Protsailo, L. V.; Fawcett, W. R. *Electrochim. Acta* **2000**, *45*, 3497−3505.
(63) Cui, X.; Jiang, D.; Diao, P.; Li, J.; Tong, R.; Wang, X. *J. Electroanal. Chem.* **1999**, *470*, 9−13.
(64) Gilbert, S. E.; Cavalleri, O.; Kern, K. *J. Phys. Chem.* **1996**, *100*, 12123−12130.
(65) Burgess, J. D.; Hawkridge, F. M. *Langmuir* **1997**, *13*, 3781−3786.
(66) Nishizawa, M.; Sunagawa, T.; Yoneyama, H. *Langmuir* **1997**, *13*, 5215−5217.
(67) Cavalleri, O.; Gilbert, S. E.; Kern, K. *Chem. Phys. Lett.* **1997**, *269*, 479−484.
(68) Cavalleri, O.; Gilbert, S. E.; Kern, K. *Surf. Sci.* **1997**, *377−379*, 931−936.
(69) Oyamatsu, D.; Nishizawa, M.; Kuwabata, S.; Yoneyama, H. *Langmuir* **1998**, *14*, 3298−3302.
(70) Zamborini, F. P.; Campbell, J. K.; Crooks, R. M. *Langmuir* **1998**, *14*, 640−647.
(71) Baker, W. S.; Crooks, R. M. *J. Phys. Chem. B* **1998**, *102*, 10041−10046.
(72) Cavalleri, O.; Kind, H.; Bittner, A. M.; Kern, K. *Langmuir* **1998**, *14*, 7292−7297.
(73) Cavalleri, O.; Bittner, A. M.; Kind, H.; Kern, K. *Z. Phys. Chem.* **1999**, *208*, 107−136.
(74) Hagenstroem, H.; Schneeweiss, M. A.; Kolb, D. M. *Electrochim. Acta* **1999**, *45*, 1141−1145.
(75) Oyamatsu, D.; Kuwabata, S.; Yoneyama, H. *J. Electroanal. Chem.* **1999**, *473*, 59−67.
(76) Hagenstrom, H.; Schneeweiss, M. A.; Kolb, D. M. *Langmuir* **1999**, *15*, 2435−2443.
(77) Hagenstrom, H.; Schneeweiss, M. A.; Kolb, D. M. *Langmuir* **1999**, *15*, 7802−7809.
(78) Schneeweiss, M. A.; Hagenstrom, H.; Esplandiu, M. J.; Kolb, D. M. *Appl. Phys. A* **1999**, *69*, 537−551.
(79) Whelan, C. M.; Smyth, M. R.; Barnes, C. J. *Langmuir* **1999**, *15*, 116−126.
(80) Hsieh, M.-H.; Chen, C.-H. *Langmuir* **2000**, *16*, 1729−1733.
(81) Baker, M. V.; Jannings, G. K.; Laibinis, P. E. *Langmuir* **2000**, *16*, 3288−3293.
(82) Hagenstrom, H.; Esplandiu, M. J.; Kolb, D. M. *Langmuir* **2001**, *17*, 839−848.
(83) Oyamatsu, D.; Kanemoto, H.; Kuwabata, S.; Yoneyama, H. *J. Electroanal. Chem.* **2001**, *497*, 97−105.
(84) Tremont, R. J.; Blasini, D. R.; Cabrera, C. R. *J. Electroanal. Chem.* **2003**, *556*, 147−158.
(85) Shimazu, K.; Kawaguchi, T.; Isomura, T. *J. Am. Chem. Soc.* **2002**, *124*, 652−661.
(86) Shimazu, K.; Hashimoto, Y.; Kawaguchi, T.; Tada, K. *J. Electroanal. Chem.* **2002**, *534*, 163−169.
(87) Esplandiu, M. J.; Hagenstrom, H. *Solid State Ionics* **2002**, *150*, 39−52.
(88) Epple, M.; Bittner, A. M.; Kuhnke, K.; Kern, K.; Zheng, W. Q.; Tadjeddine, A. *Langmuir* **2002**, *18*, 773−784.
(89) Lin, S.-Y.; Tsai, T.-K.; Lin, C.-M.; Chen, C.-H. *Langmuir* **2002**, *18*, 5473−5478.
(90) Kongkanand, A.; Kuwabata, S. *Electrochem. Commun.* **2003**, *5*, 133−137.
(91) Blasini, D. R.; Tremont, R. J.; Batine, N.; Gonzalez, I.; Cabrera, C. R. *J. Electroanal. Chem.* **2003**, *540*, 45−52.
(92) Wanunu, M.; Vaskevich, A.; Rubinstein, I. *J. Am. Chem. Soc.* **2004**, *126*, 5569−5576.
(93) Hepel, M.; Tewksbury, E. *Electrochim. Acta* **2004**, *49*, 3827−3840.
(94) Vergheese, T. M.; Berchmans, S. *Mater. Chem. Phys.* **2004**, *83*, 229−238.
(95) Herzog, G.; Arrigan, D. W. M. *Electroanalysis* **2005**, *20*, 1816−1821.
(96) Kolb, D. M. In *Advances in Electrochemistry and Electrochemical Engineering*; Gerischer, H., Tobias, C. W., Eds.; Wiley-Interscience: New York, 1978; Vol. 11, pp 125−271.
(97) Juttner, K.; Lorenz, W. J. *Z. Phys. Chem. (Wiesbaden)* **1980**, *122*, 163−185.
(98) Adzic, R. In *Advances in Electrochemistry and Electrochemical Engineering*; Gerischer, H., Tobias, C. W., Eds.; Wiley-Interscience: New York, 1984; Vol. 13, pp. 159−260.

impedes diffusion of the metal cation to the electrode surface for reduction. For SAMs formed from alkanethiols, the degree of this inhibition has been found to be a function of alkanethiol chain length.[87,88] Moreover, substantial changes in alkanethiol orientation have been observed by vibrational sum-frequency generation during Cu UPD on a hexanethiol SAM-covered Au (111) electrode.[88] This orientational change was found to be a sensitive function of chain length, with dodecanethiol SAMs showing only partial reorientation, and octadecanethiol showing no reorientation.[88]

Cabrera and co-workers have reported Pb UPD at Cu surfaces modified with propanethiol, propyltrimethoxysilane, and 3MPT SAMs[84] and at iodine-coated Au surfaces modified with 3MPT SAMs.[91] Shimadzu also used Pb UPD to investigate mixed monolayers of mercaptopropionic acid and alkanethiols on Au.[86] To date, only Yoneyama and co-workers have compared the UPD behavior of multiple metals at the same SAM-coated electrode.[75] From a study of the UPD behavior of Tl, Pb, Ag, Cd, Cu, and Bi at propanethiol- and octanethiol-coated Au electrodes, these researchers concluded that the ability of a metal ion to penetrate the SAM alkyl region is directly correlated to its Stokes diameter. This study effectively demonstrated the advantages of using multiple UPD metal probes to examine a particular SAM.

Although most previous UPD studies with SAMs have been performed on Au substrates, the UPD of Pb[99,100] and Tl[100,101] are well-known at Ag surfaces. Of the previously reported studies, none has explored the perturbation of polymerizable SAM systems by underpotential metal deposition. The work reported here seeks to elaborate on the initial study of Pb UPD on 3MPT-modified Ag electrodes reported from this laboratory, in which complete blocking of Pb UPD in aqueous Cl^- solution was observed.[22] By examining the UPD behavior of two additional metals—Tl and Cd—and comparing and contrasting their UPD characteristics to that of Pb, a more detailed understanding of the structure of the 3MPT SAM is deduced.

Experimental

Materials. 3MPT (Aldrich, >98%) was vacuum distilled prior to use. Butanethiol (BT; Aldrich, 99%) was used as received. Reagent-grade acids (Mallinckrodt; HCl, HNO_3, H_2SO_4, and $HClO_4$) were used as received. Anhydrous 100% ethanol was obtained from Midwest Grain Products or McCormick and used immediately after opening. $Pb(NO_3)_2$, Tl_2SO_4, and $CdSO_4$ were reagent grade (Alfa AESAR) and used as received. K_2SO_4 (Baker, reagent grade) and $KClO_4$ (Aldrich, 99+%) were used as received. Water was obtained from a Milli-Q UV Plus ultrapure Millipore water system (18.2 MΩ cm; <10 ppb total organic carbon).

Polycrystalline Ag disks (Johnson Matthey, 99.999%) were mechanically polished with 400−1500 grit SiC sandpaper (3M) and a 5 μm Al_2O_3 slurry (Buhler, Ltd.) The sides of the polished surfaces were then wrapped with Parafilm and placed into concentrated $HClO_4$ for 5−10 min. The surfaces were then immediately transferred to a polishing solution of 3−4 M CrO_3 and 0.6 M HCl. This solution was gently stirred for ∼1 min. The surfaces were then rinsed with copious amounts of Milli-Q water and immersed into concentrated NH_4OH for ∼1−5 min. The surfaces were then rinsed with Milli-Q water and dipped into fresh concentrated $HClO_4$, rinsed again with Milli-Q water and then anhydrous ethanol, and stored under dry ethanol prior to use.

SAMs were prepared by the immersion of freshly prepared Ag substrates into 20 mM solutions of either 3MPT or BT in dry ethanol. For BT SAMs, self-assembly was allowed to progress for 12 h followed by rinsing with dry ethanol and drying in a stream of nitrogen gas. For 3MPT SAMs, self-assembly was allowed to progress for 2 h, and the surfaces were rinsed with dry ethanol followed by immersion into a solution of 0.1 M HCl for 1−12 h to hydrolyze and condense the trimethoxy headgroups.[22]

Electrochemistry. Cyclic voltammetry was performed using a BAS 100B workstation. For all experiments, a three-electrode electrochemical cell was employed using a Pt wire counter electrode and a Ag/AgCl reference electrode (saturated KCl).

UPD solutions of 1 mM Tl_2SO_4/0.1 M K_2SO_4/2 mM H_2SO_4, 1 mM $Pb(NO_3)_2$/0.1 M $NaClO_4$/2 mM $HClO_4$, and 1 mM $CdSO_4$/0.1 M K_2SO_4/2 mM H_2SO_4 were purged for 20 min with water-saturated N_2 prior to use. A positive pressure of N_2 was maintained in the electrochemical cell during the experiments.

Emersion Raman Spectroscopy. Raman spectral data were collected on an instrument described previously based on a Spex 270M single monochromator with a 1200 gr/mm grating blazed at 630 nm. Detection was accomplished with a Tektronix TK-512T, 512 × 512 thinned, back-illuminated CCD system (Princeton Instruments). A holographic Super Notch Plus filter (Kaiser Optical Systems) was used to reduce the background from the Raleigh scattered light. Integration times were 10 s co-added 60 times for a total of 10 min to achieve a reasonable signal-to-noise level, with p-polarized 514.5 nm light from a Coherent Innova 300c Ar^+ laser with 70 mW incident on the sample at ∼40° from the surface normal unless otherwise noted. Scattered light was collected at ∼50° from the surface normal.

Recent publications have described the emersion geometry for spectroscopy;[102−105] thus, it will be described only briefly here. For Raman spectroscopy in the emersion configuration, the cell is made of pyrex glass and sealed with a Teflon lid. An inert atmosphere with saturated water vapor is maintained in the cell by a flowing stream of water-saturated N_2 through the cell. A capillary of ∼1 mm i.d. is used to bring electrolyte to the lower portion of the surface, where a droplet of the UPD electrolyte extending from the capillary to the working electrode surface defines the electrochemical cell. A Ag wire quasi-reference electrode (AgQRE; potential ∼ −0.14 V vs Ag/AgCl) is immersed into the droplet to minimize the uncompensated resistance. The working electrode is connected to a motor that slides through a Teflon sheath in a ground-glass joint on the side of the cell. Electrical contact with the working electrode was made through a graphite brush. Electrode potentials were controlled with an EG&G model 283 potentiostat.

Emersion of the 3MPT-modified Ag was achieved by rotation of the surface through an electrolyte drop extruded from a capillary using a miniature DC motor (DynaOptic Motion) at 0.013 mm/s. Spectra were acquired with the focused laser spot positioned 1 mm down from the top of the surface.

Molecular Mechanics Energy Minimization Computations. Energy-minimized molecular mechanics computations were performed on CHEM 3D Ultra version 10.0 (CambridgeSoft Corp.). 3MPT/Ag structures were built using standard parameters available in Chem3D and then energy minimized to root mean square gradient values of 0.001, holding the Ag surface structure and the edge 3MPT molecules stationary. Spheres for Tl^+, Pb^{2+}, and Cd^{2+} were superimposed on these energy-minimized structures with sizes equivalent to their Stokes (hydrated) diameters.

Results and Discussion

Tl, Pb, and Cd UPD Behavior at 3MPT-Modified Ag. Figure 1 shows the cyclic voltammetry of Tl deposition at bare and 3MPT-modified Ag electrodes. These voltammograms were obtained at a relatively slow potential sweep rate of 10 mV/s to allow fine structure in the response to be resolved. Tl is a

(99) Bewick, A.; Thomas, B. *J. Electroanal. Chem.* **1977**, *84*, 127−140.
(100) Toney, M. F.; Gordon, J. G.; Samant, M. G.; Borges, G. L.; Melroy, O. R. *J. Phys. Chem.* **1995**, *99*, 4733−4744.
(101) Bewick, A.; Thomas, B. *J. Electroanal. Chem.* **1975**, *65*, 911−931.
(102) Woelfel, K. J.; Pemberton. J. E. *J. Electroanal. Chem.* **1998**, *456*, 161−169.
(103) Shen, A. J.; Pemberton, J. E. *J. Electroanal. Chem.* **1999**, *479*, 32−42.
(104) Schoenfisch, M. H.; Pemberton, J. E. *Langmuir* **1999**, *15*, 509−517.
(105) Tiani, D. J.; Pemberton, J. E. *Langmuir* **2003**, *19*, 6422−6429.

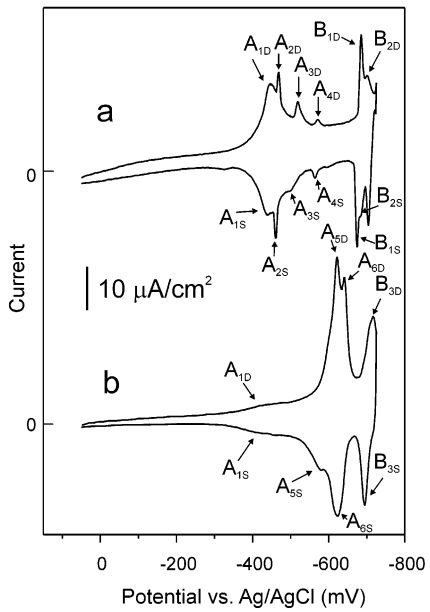

Figure 1. Voltammetry in 1 mM Tl_2SO_4/0.1 M K_2SO_4/2 mM H_2SO_4 at a potential sweep rate of 10 mV/s on (a) Ag and (b) 3MPT-modified Ag surfaces. The potential window terminates at the foot of reversible bulk Tl deposition.

Table 1. Voltammetric Peak Potentials (10 mV/s) for UPD Tl at Bare and 3MPT-Modified Ag

	bare Ag (mV)[a]		3MPT-modified Ag (mV)[b]	
peak	deposition	stripping	deposition	stripping
$A_{1D/1S}$	−445	−438	−445[c]	−420[c]
$A_{2D/2S}$	−472	−467		
$A_{3D/3S}$	−519	−512		
$A_{4D/4S}$	−572	−566		
$B_{1D/1S}$	−690	−683		
$B_{2D/2S}$	−701	−704		
$A_{5D/5S}$			−621	−577
$A_{6D/6S}$			−641	−622
$B_{3D/3S}$			−716	−705
$\Delta E_{p(A1D/1S)}$	7		25	
$\Delta E_{p(A2D/2S)}$	5			
$\Delta E_{p(A3D/3S)}$	7			
$\Delta E_{p(A4D/4S)}$	6			
$\Delta E_{p(B1D/1S)}$	7			
$\Delta E_{p(B2D/2S)}$	3			
$\Delta E_{p(A5D/5S)}$			44	
$\Delta E_{p(A6D/6S)}$			19	
$\Delta E_{p(B3D/3S)}$			11	

[a] Standard deviations for three independent Ag surfaces are less than 0.01 V. [b] Standard deviations for three independent 3MPT-modified Ag surfaces are less than 0.01 V. [c] These peak potentials in the presence of 3MPT acquired at a sweep rate of 100 mV/s.

particularly interesting probe because of the remarkable sensitivity of its UPD to different crystal faces of Ag.[100,101] In Figure 1a, the voltammogram is initiated at 50 mV and swept toward more negative potential through deposition of the first (peaks A_{1D}−A_{4D}) and second (peaks B_{1D}−B_{2D}) Tl monolayers prior to the onset of bulk Tl deposition at approximately −705 mV. When the direction of potential sweep is reversed, the second and first monolayers are subsequently stripped at potentials nearly identical to those at which they were deposited (peaks B_{1S}−B_{2S} and A_{1S}−A_{4S}, respectively).[101] Peak potentials are tabulated in Table 1.

Bewick and Thomas previously investigated the voltammetric UPD signatures for Tl on Ag (100), Ag (110), and Ag (111) electrodes.[99] On the basis of the voltammogram in Figure 1a, the Ag electrodes used here exhibit a significant fraction of Ag (110)

Table 2. UPD Stripping Charge at Bare and 3MPT-Modified Ag Electrodes

system	UPD Tl (μC/cm^2)[a]	UPD Pb (μC/cm^2)[a]	UPD Cd (μC/cm^2)[b]
bare Ag	360 ± 50	600 ± 40	300 ± 200
3MPT/Ag (major)	360 ± 70	404 ± 20	NO[c]
3MPT/Ag (defects)	50 ± 10	60 ± 5	NO
3MPT/Ag (total)	400 ± 70	460 ± 30	NO

[a] Standard deviations for five surfaces. [b] Standard deviation for three surfaces. [c] NO = not observed.

behavior in the response, with a large, broad wave at −445 mV and smaller, sharper peaks at −472, −519, and −572 mV for A_{2D}, A_{3D}, and A_{4D}, respectively. Although each of the low-index crystal faces have different UPD signatures[99] (i.e., peak potentials, peak widths, etc.), the voltammetry exhibits too much overlap of the single-crystal surfaces to quantitatively determine the fraction of each crystal lattice on these electrodes. Additional complexity in these voltammograms results from the polycrystalline nature of the substrate with grain boundaries not present on single-crystal surfaces.

Figure 1b shows the voltammetry for Tl UPD at these Ag electrodes when covered by a hydrolyzed and cross-linked monolayer of 3MPT. The initial expectation was that the 3MPT layer would completely block Tl monolayer deposition in a manner similar to that previously observed for Pb UPD.[22] However, although in the presence of 3MPT, the potential at which Tl UPD occurs changes (Figure 1b and Table 1), on the basis of the peak separation between the deposition (A_{5D}, A_{6D}, B_{3D}) and stripping waves (A_{5S}, A_{6S}, B_{3S}), the UPD process does not appear to be unduly inhibited by kinetic (mass transport) effects in the presence of the SAM and resembles the process on bare Ag. *Indeed, the relatively facile UPD of a metal in the presence of a thiol-based monolayer as demonstrated in Figure 1b is without precedent in the previous literature.*

The stripping charge for each UPD process referred to above is given in Table 2. In the presence of the 3MPT monolayer, a small wave corresponding to ∼8−12% of the total surface area is present at the potential of A_{1D} (−445 mV). This wave is attributed to Tl UPD at film defects not covered by 3MPT. However, the major portion of the Tl UPD peak (A_{1D}) at −445 mV shifts to −621 mV (A_{5D}), with a second, smaller UPD peak observed at −641 mV (A_{6D}). Peaks for the deposition of the second monolayer (peaks B_{1D}−B_{2D} on bare Ag) are also shifted to more negative potentials at the 3MPT-modified surface, but are reduced to a single broad peak (B_{3D}).

The integrated charge under the wave for UPD of the first Tl monolayer on 3MPT-modified Ag accounts for ∼90% of the surface area of the underlying Ag. The presence of these peaks at potentials more positive than the standard reduction potential indicates that UPD still occurs. Moreover, the total integrated charge for deposition (or stripping) of the first Tl monolayer on the 3MPT-modified Ag surface (including Tl deposited in defect regions) is identical to that on bare Ag, indicating that a full UPD monolayer is formed. Thus, the first Tl monolayer must deposit in intimate contact with the underlying Ag electrode *beneath the 3MPT layer*.

Film defects arise from incomplete coverage of the Ag surface by 3MPT. The size of defects in 3MPT films prepared by different methods has been reported to be on the order of several tens of nanometers.[84] A previous study of 3MPT films on Cu substrates showed similar values (∼3−10%) of surface area associated with film defects. Pt was found to electrochemically deposit (not at underpotential) from a solution containing $PtCl_6^{2-}$ onto the Cu surface within these defects at the same potential as on bare

Cu.[84] The observation of Tl UPD on 3MPT-modified Ag in the identical potential regime wherein it occurs on bare Ag (i.e., between approximately −400 and −550 mV) is consistent with this observation.

Differences in the voltammetric behavior for Tl UPD on 3MPT-modified Ag electrodes compared to that on bare Ag can be attributed largely to thermodynamic effects arising from the presence of the 3MPT layer. However, as will be discussed in greater detail below, slight kinetic complications to the Tl UPD process are also indicated by the voltammetry. The 176 mV shift to more negative potentials of the primary UPD peak for the first Tl monolayer results from a decrease in thermodynamic advantage for Tl UPD on the 3MPT-modified Ag surface relative to bare Ag due to the need to break the strong Ag-3MPT bond before forming the Ag−Tl and Tl-3MPT bonds. In addition, the number of peaks in the voltammogram decreases from four (A_{1D}−A_{4D}) to two (A_{5D}−A_{6D}), suggesting that the 3MPT-modified Ag is thermodynamically more uniform compared with the bare Ag surface. Assuming that the two-dimensionally polymerized 3MPT layer rebinds to the first Tl layer deposited at underpotential, the small negative shift of 26 mV for deposition of the second Tl monolayer indicates that the energy loss incurred from breaking the Ag−S bond to deposit the first monolayer is significantly greater than the energy loss incurred to break the Tl−S bond during deposition of the second Tl monolayer.

Examination of the potential separation between the deposition and stripping peaks (ΔE_p in Table 1) for the first Tl monolayer demonstrates another difference between 3MPT-modified and bare Ag. At a potential sweep rate of 10 mV/s, ΔE_p for deposition of the first Tl monolayer on bare Ag (ΔE_{pA1} in Table 1) is 7 mV, but for deposition of the first Tl monolayer on 3MPT-modified Ag (ΔE_{pA5}), it increases to 44 mV. Similarly, ΔE_{pA2} between A_{2D} and A_{2S} on bare Ag is 5 mV, whereas ΔE_{pA6} between A_{6D} and A_{6S} in the presence of 3MPT is 19 mV. Slightly larger values of ΔE_p are observed on 3MPT-modified Ag at 25 mV/s (data not shown.) The consistent increase in ΔE_p in the presence of the 3MPT layer suggests a slight kinetic limitation in the deposition and stripping of the Tl monolayer relative to these processes at bare Ag. The presence of tailing on the monolayer stripping wave (A_{5S}) in the presence of 3MPT lends additional support to the presence of kinetic complications. Similar tailing is not observed on either side of the deposition wave at 3MPT-modified Ag, suggesting that these kinetic complications are associated with the injection of Tl^+, created by the oxidation of UPD Tl°, into solution.

Although kinetic limitations due to the inhibition of mass transport are suggested by the increase in peak separation for the 3MPT-modified surface, these effects are relatively small under the conditions of this study. This behavior is consistent with the previous observation of Yoneyama for Tl UPD at propanethiol-modified Au surfaces in which almost identical peak separations in the presence (100 mV) and absence (90 mV) of the monolayer were observed,[75] but is quite different from that observed for other UPD systems using larger metal cations at SAMs of similar thickness formed from short-chain alkanethiols.[66,69,74,77,82] For example, Hagenstrom and co-workers[74] reported an increase in ΔE_p from ∼50 to ∼600 mV for Cu UPD at ethanethiol-modified Au relative to bare Au at 10 mV/s. Similarly, for Cu UPD, Yoneyama and co-workers report an increase in ΔE_p from 81 mV at bare Au to 545 mV at a propanethiol-modified Au electrode at 2 mV/s.[66,75] These increases in ΔE_p were attributed to the presence of an additional impedance from a kinetic barrier associated with penetration of the SAM by Cu^{2+}. Thus, in contrast to the observed dominance of thermodynamic effects for Tl UPD on 3MPT-modified Ag reported here (with superimposed minor kinetic effects), Hagenstrom et al. and Yoneyama et al. found that kinetic limitations dominate Cu UPD on ethanethiol- and propanethiol-modified Au, respectively. On the basis of these differences, one must conclude that the rather striking difference in behavior between Tl UPD at 3MPT-modified Ag and systems with larger cations at alkanethiol SAMs similar in layer thickness must arise from some structural feature of the 3MPT monolayer.

3MPT films are known to have a considerably lower packing density than SAMs formed from alkanethiols due to the presence of the bulky trimethoxy groups.[22,106,107] The diameter of the trimethoxysilane terminus is almost 70% larger than that of a methyl terminal group (∼0.65 nm compared to ∼0.39 nm), creating additional space between thiol molecules during film formation. Thus, upon hydrolysis and condensation of the trimethoxysilane terminus to form a two-dimensionally polymerized siloxane structure,[22,106] the propyl chains of the 3MPT are spaced much farther apart than in an alkanethiol film. Several experimental approaches have provided evidence that the siloxane-linked structure is largely complete, with only a small percentage of chemically accessible free silanol groups left on the surface of the SAM. This structure is consistent with calculations[106] of a 3MPT layer on Au (111) that indicate a probable siloxane-linked structure consisting of predominantly six-membered siloxane rings ∼0.5 nm in diameter. This structure is also consistent with what is known about the structure of β-cristabolite (111) or trydimite surfaces in which the Si−Si distance in six-membered rings on the surface is 0.32 nm.[108] Such a structure is only ∼10% larger than the typical Ag−Ag spacing of 0.29 nm in Ag (111). Thus, the outer edge of this layer is predicted to look very similar to a sheet silicate structure. Indeed, this predicted structure is remarkably similar to that reported on the basis of STM studies of 3MPT-modified Au (111) in which the presence of uniform rings 0.5−0.7 nm in diameter was observed.[109] A similar structure for the 3MPT monolayer on Ag is assumed here. Depending on the angle of the siloxane bond, allowing for some ring pucker in this angle to accommodate these rings to the underlying Ag lattice through the coupled propylsilane moiety, and considering the van der Waals radii of Si and O, such a structure would leave ∼0.25−0.30 nm of free space in the center of the six-membered ring through which Tl^+, even fully hydrated (Stokes diameter 0.246 nm[75]), could easily pass to access the underlying Ag surface. It should be noted that Yoneyama and co-workers demonstrated a clear dependence on *hydrated ion size* through the Stokes diameter, not crystal ion size, for UPD on propanethiol- and octanethiol-modified Au electrodes.[75] Although the implications of these points are discussed in further detail below, the structural model described above allows a crude level of predictability for which metal ions might readily access the underlying Ag substrate through the 3MPT layer, and thereby undergo relatively unimpeded UPD, as opposed to reduction only at SAM defects[66,69,77,82] or only at the outer edge of the SAM by tunneling,[64,67,68] as has been previously proposed for electrochemical metal deposition through SAMs formed from normal alkanethiols. In order to further test this hypothesis, the UPD processes for Pb^{2+} (Stokes diameter 0.266 nm[75]) and Cd^{2+} (Stokes diameter 0.342 nm[75]) were also investigated. On the basis of the above model, one would predict that Pb^{2+} should exhibit relatively

(106) Mihailova, B.; Engstrom, V.; Hedlund, J.; Sterte, J. *J. Mater. Chem.* **1999**, *9*, 1507−1510.
(107) Wang, Y.; Yu, Q.; Zhang, Y.; Guo, Z.; Gu, N.; Wesche, K. D. *Appl. Surf. Sci.* **2004**, *229*, 377−386.
(108) Stevens, M. J. *Langmuir* **1999**, *15*, 2773−2778.
(109) Che, G.; Manivannan, A.; Cabrera, C. R. *Physica A* **1996**, *231*, 304−316.

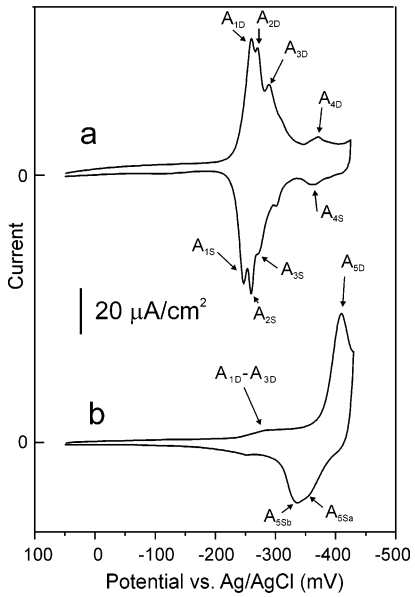

Figure 2. Voltammetry in 1 mM $Pb(NO_3)_2$/0.1 M $NaClO_4$/2 mM $HClO_4$ at a potential sweep rate of 10 mV/s on (a) Ag and (b) 3MPT-modified Ag surfaces. The potential window terminates at the foot of reversible bulk Pb deposition.

Table 3. Voltammetric Peak Potentials (10 mV/s) for UPD Pb at Bare and 3MPT-Modified Ag

	bare Ag (mV)[a]		3MPT-modified Ag (mV)[b]	
peak	deposition	stripping	deposition	stripping
$A_{1D/1S}$	−260	−245	−270	−250
$A_{2D/2S}$	−271	−257	−270	−250
$A_{3D/3S}$	−288	−272	−270	−250
$A_{4D/4S}$	−320	−303		
$A_{5D/5S}$	−370	−362		
$A_{6D/6S}$			−414	−335, −345
$\Delta E_{p(A1D/1S)}$	15		20	
$\Delta E_{p(A2D/2S)}$	15			
$\Delta E_{p(A3D/3S)}$	16			
$\Delta E_{p(A4D/4S)}$	17			
$\Delta E_{p(A5D/5S)}$	8			
$\Delta E_{p(A6D/6S)}$			69, 79	

[a] Standard deviations for three independent Ag surfaces are less than 0.01 V. [b] Standard deviations for three independent 3MPT-modified Ag surfaces are less than 0.01 V.

facile UPD behavior, while that for Cd^{2+} should be considerably more inhibited by the presence of the 3MPT layer.

Figure 2 shows the cyclic voltammetry for UPD Pb at bare Ag and 3MPT-modified Ag electrodes. Peak potentials are tabulated in Table 3 and the UPD charge in Table 2. The deposition of Pb differs from that of Tl in that the second monolayer does not begin to deposit before the onset of bulk deposition. In the voltammogram at bare Ag, four distinct peaks are observed for deposition and stripping processes in the underpotential region. The deposition peaks corresponding to the first monolayer (A_{1D}−A_{5D}) are observed at −260, −271, −288, −320, and −370 mV, respectively. A_{1D}−A_{4D} fall within a large envelope dominated by A_{1D}. These peaks are due to Pb deposition on multiple sites on the Ag surface (i.e., atomic step-edges, plateaus, or different crystal faces).[99−101] In the presence of 3MPT, A_{1D} is largely eliminated, although a small wave corresponding to ∼10% of the original surface area is still observed due to Pb UPD at 3MPT film defects. In addition, a new peak develops at −414 mV (A_{6D}) due to Pb UPD beneath the 3MPT monolayer. Since the thermodynamic advantage for Pb UPD is not as large as that for Tl UPD, this peak is not fully resolved at the switching potential. Upon scan reversal, a stripping wave is observed that has two components at −345 and −334 mV (A_{6Sa} and A_{6Sb}, respectively.) As for Tl, the presence of a UPD peak at the 3MPT-modified electrode indicates that Pb is deposited in direct contact with the Ag surface beneath the 3MPT layer.

The most significant difference between Pb and Tl UPD at 3MPT-modified Ag is the value of ΔE_p. For Pb UPD at bare Ag, ΔE_{pA1} (see Table 2) is 15 mV, indicating little to no kinetic limitation. In contrast, for Pb UPD at 3MPT-modified Ag, ΔE_{pA6} increases to 79 mV for the stripping peak, suggesting an additional kinetic limitation to the Pb deposition and stripping processes. The magnitude of this kinetic effect for Pb UPD (79 mV) is significantly larger than that for Tl UPD (44 mV) at 3MPT-modified Ag. Thus, Pb UPD is more kinetically inhibited than Tl UPD, suggesting that its size is approaching the limit of that easily accommodated by the open space in the six-membered siloxane rings at the outer edge of the 3MPT monolayer. The crystal ionic diameter of Pb^{2+} (0.266 nm[110]) is almost 20% smaller than that of Tl^+ (0.328 nm[110]). Therefore, if crystal ionic size were the determinant in ion accessibility to the underlying Ag surface, one would predict a smaller kinetic limitation for Pb UPD than for Tl UPD. This is clearly not observed. On the other hand, the hydrated Stokes diameter of Pb^{2+} (0.266 nm[75]) is ∼8% larger than that of Tl^+ (0.246 nm[75]). Although only a small difference, the hydrated Pb^{2+} size is comparable to or slightly exceeds the 0.25−0.30 nm diameter ring openings in the expected 3MPT structures (see below) and therefore might be subject to slight kinetic inhibition of ion penetration.

Alternately, the observed impact of the 3MPT layer on the kinetics of Pb monolayer deposition could indicate that the bridging of the polymerized 3MPT layer across regions of the Ag surface that are bare and those that contain islands of a growing Pb monolayer is not as energetically favorable as with a growing Tl monolayer. Regardless of the cause of the slightly greater kinetic inhibition observed for Pb UPD relative to Tl UPD, the process for Pb UPD is thought to occur mechanistically in much the same way as that for Tl at 3MPT-modified Ag electrodes. This result is expected on the basis of the similarity in Stokes diameters of the two ions and the covalent diameters of the two metal atoms (Tl 0.342 nm, Pb 0.350 nm[111]).

Figure 3 shows the voltammetry for Cd UPD at bare Ag and 3MPT-modified Ag electrodes. At bare Ag (Figure 3a), Cd UPD begins at approximately −315 mV with deposition peaks A_{1D}−A_{5D} at −407, −450, −474, −625, and −645 mV, and their associated stripping peaks A_{5S}−A_{1S} at −633, −590, −473, −444, and −407 mV, respectively. All components of the stripping wave are nearly symmetric with those for deposition (i.e., ΔE_p ∼ 0 mV.) Cd UPD differs from Tl and Pb UPD in that deposition of the first monolayer occurs in two steps: a broad pre-UPD nucleation region encompassing A_{1D}−A_{3D} maximizing at −474 mV, and a sharp UPD envelope encompassing peaks A_{4D} and A_{5D} at approximately −650 mV.[112] The integrated charge associated with A_{1D}−A_{3D} is ∼300 μC/cm^2, which is ∼38% of the full Cd monolayer, whereas the charge associated with peaks A_{4D} and A_{5D} is ∼511 μC/cm^2, corresponding to the remainder of the full monolayer. It should be noted, however, that a Cd−Ag alloy can be formed during the UPD of Cd on Ag,[112] especially if the potential is held for even shorter periods of time within the underpotential regime. Although this alloy formation is fully reversible when the Cd is stripped from the surface, the complexity

(110) Shannon, R. D. *Acta Crystallogr., Sect. A* **1976**, *32*, 751−767.
(111) Shackelfork, J., Alexander, W., Eds. *CRC Materials Science and Engineering Handbook*; CRC Press: Boca Raton, FL, 1992.
(112) Bort, H.; Juttner, K.; Lorenz, W. E. *Electrochim. Acta* **1978**, *28*, 993−1001.

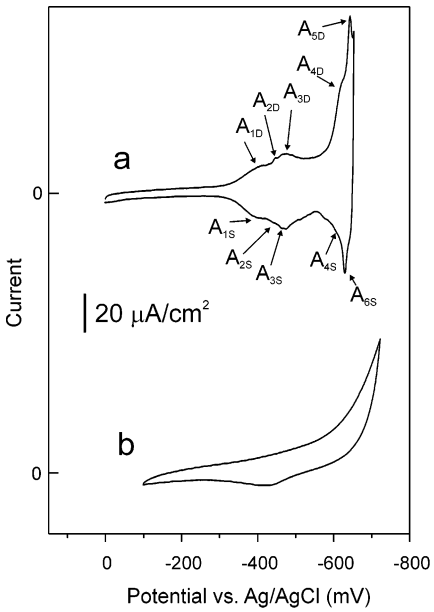

Figure 3. Voltammetry in 1 mM $CdSO_4$/0.1 M K_2SO_4/2 mM H_2SO_4 at a potential sweep rate of 10 mV/s on (a) Ag and (b) 3MPT-modified Ag surfaces. The potential window terminates at the foot of reversible bulk Cd deposition.

of the Cd UPD voltammetry on Ag may represent a small contribution from alloy formation at the potential sweep rate of 10 mV/s of this study.

At the 3MPT-modified surface (Figure 3b), current onset begins at approximately −600 mV with no discrete peak apparent. In the stripping portion of the voltammogram, a small, broad peak appears at −425 mV, the potential at which the first 38% of a UPD Cd monolayer on bare Ag is stripped. When integrated, this peak encompasses 128 $\mu C/cm^2$ of charge, corresponding to ∼16% of a full Cd monolayer. This area is larger than the estimated defect area of 3MPT-modified Ag surfaces based on electrochemical impedance measurements[113] (not shown) and based on the fractional defect density from the Tl and Pb UPD behavior discussed above. Therefore, although no discrete UPD wave for Cd deposition is observed, a fraction of the first monolayer of Cd deposits on the Ag surface in the underpotential regime, albeit with severe kinetic limitations. The lack of significant observable UPD activity for Cd in this system presumably results from steric inhibition of the penetration of hydrated Cd^{2+} by the outer siloxane cross-linked terminus of 3MPT as predicted above.

Mechanism for Metal UPD at 3MPT-Modified Ag. On the basis of the voltammetric results discussed above, the mechanism shown in Figure 4 for metal UPD at 3MPT-modified Ag is proposed. Figure 4a shows the 3MPT layer prior to UPD of a foreign metal layer. Although the true nature of the defect sites within the 3MPT layer is unknown, two defects are depicted simply as 3MPT vacancies. These sites are proposed to serve as the primary nucleation sites for the growth of islands of the monolayer metal (Figure 4b), although the penetrability of the 3MPT layer by both Tl^+ and Pb^{2+} must result in a large number of smaller growing islands in these cases as well. As the UPD process continues, these islands extend outward by two-dimensional growth of the metal monolayer beneath the 3MPT-covered portions of the electrode surface as shown in Figure 4c until the monolayer beneath the 3MPT is complete (Figure 4d). This two-dimensional growth mechanism requires that the 3MPT

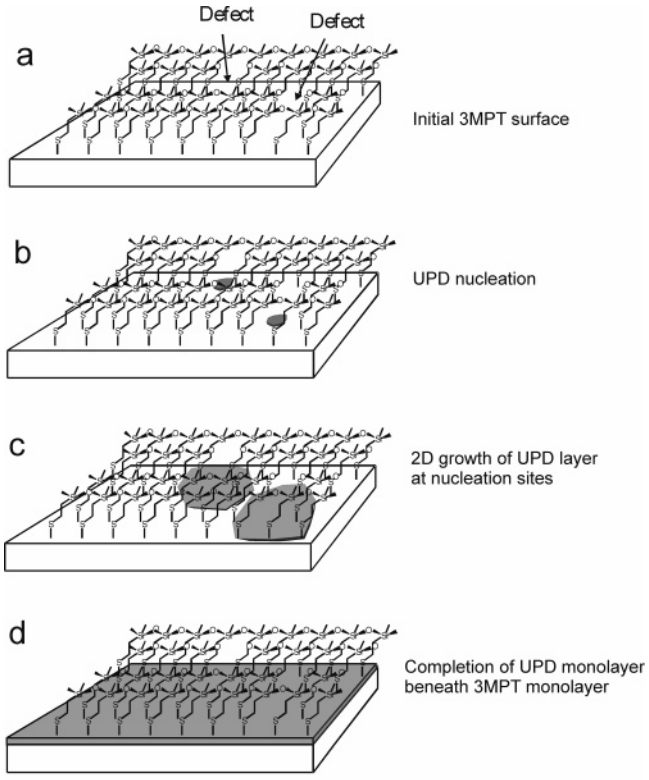

Figure 4. Schematic representation of the UPD process at a 3MPT-modified Ag surface.

layer break its bonds with the Ag surface and "step-up" onto the growing metal monolayer. During intermediate periods of monolayer growth when the surface is only partially covered with the metal monolayer, the 3MPT layer must span regions of the surface that are both bare and covered by the metal. Varying amounts of strain will be induced into the two-dimensionally siloxane-linked 3MPT layer at regions of the surface where it transitions from bare to metal-covered regions. The introduction of this strain could be an additional contribution leading to the slower kinetics of deposition for the first Pb monolayer compared to Tl.

The observation that both Tl and Pb can be deposited at underpotential, while Cd can not, strongly suggests a dependence on the Stokes diameter of the metal cation. The fact that UPD is observed at defect sites for all three metals indicates that two-dimensional growth of the metal monolayer beneath 3MPT is not limited by the supply of metal cations to the outer edges of growing metal islands.

This picture is supported by molecular modeling using energy-minimized molecular mechanics computations of the predicted 3MPT ring structures on the three low-index crystal faces of Ag. Figure 5 shows molecular pictures of these structures with the Stokes diameters of each of the three metal cations studied here superimposed over a ring opening. The ring structures that can be accommodated on each of the three crystal faces are slightly different, but exhibit bond angles and lengths well within the previously observed range (120−180°) for the inherently flexible siloxane linkage in vitreous silica[114−118] and simple organosilane compounds.[119−121] Specifically, in the 3MPT structure in Figure

(113) Robertson, J. W. F. Ph.D. Dissertation, University of Arizona, Tucson, AZ, 2004.

(114) Mozzi, R. L.; Warren, B. E. *J. Appl. Crystallogr.* **1969**, *2*, 164−172.
(115) Leadbetter, A. J.; Wright, A. C. *J. Non-Cryst. Solids* **1972**, *7*, 141−155.
(116) Garofalini, S. H. *J. Chem. Phys.* **1983**, *78*, 2069−2072.
(117) Mauri, F.; Pasquarello, A.; Pfrommer, B. G.; Yoon, Y. G.; Louie, S. G. *Phys. Rev. B* **2000**, *62*, R4786−R4789.
(118) Litton, D. A.; Garofalini, S. H. *J. Appl. Phys.* **2001**, *89*, 6013−6023.

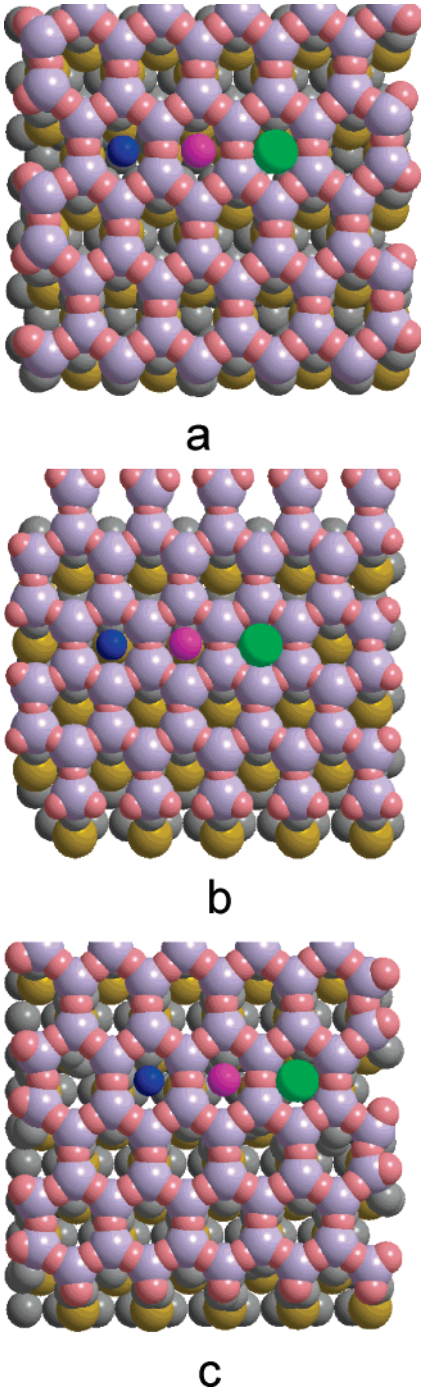

Figure 5. Energy-minimized molecular mechanics computation results for hydrolyzed and cross-linked 3MPT-modified Ag for (a) Ag (110), (b) Ag (111), and (c) Ag (100). Stokes diameters of metal ions shown superimposed over siloxane ring openings were added after minimization. Color scheme: gray = Ag, gold = S, dark gray = C, lavender = Si, pink = O, blue = Tl^+, fuchsia = Pb^{2+}, green = Cd^{2+}. Hydrogen atoms not shown but are included in minimization.

5a on Ag(110), the S atoms bond in atop and long bridge sites, yielding slightly elongated siloxane rings with long Si−O−Si distances and angles averaging[121] 0.407 nm and 152°, and short Si−O−Si distances and angles averaging 0.355 nm and 142°, respectively. For Ag (111) (Figure 5b), the 3MPT S atoms bind in atop and 3-fold sites, yielding symmetric siloxane rings with Si−O−Si distances and angles averaging 0.340 and 154°, respectively. 3MPT S atoms bind in either all atop or all bridge sites on Ag (100) (Figure 5c), giving siloxane rings with average Si−O−Si distances and angles of 0.362 nm and 161°, respectively.

The overall energetics associated with the UPD of the metals considered here is a complex interplay of thermodynamic effects, as manifested in E_p values, and kinetic effects, as manifested in ΔE_p values. The data above clearly support the varying importance of kinetic effects resulting from different degrees of steric inhibition of the hydrated metal cation in penetrating the 3MPT film. The primary thermodynamic effect suggested by the data for Tl and Pb UPD is the loss of a fraction of the underpotential stabilization energy for metal monolayer deposition on bare Ag by the need to break the Ag−S bond associated with the 3MPT SAM. However, other more subtle thermodynamic effects may also contribute. Once the 3MPT film is bonded to the metal monolayer, lateral strain that would be predicted to differ between metal monolayer systems might be engendered within the 3MPT overlayer by two effects. First, as the metal monolayer grows, the 3MPT monolayer must transition from bonding to regions of bare Ag to bonding to regions covered by the growing metal monolayer. This transition will be dynamic as metal deposition proceeds and requires that the 3MPT layer "step up" in order to bond to the growing metal monolayer. For a Ag−S bond of ∼0.3 nm,[122] this step will be the largest for Pb (diameter 0.350 nm) and Tl (diameter 0.342 nm) and the smallest for Cd (diameter 0.290 nm[111]). Given that this order is opposite the observed energetics of metal UPD based on the voltammetry described here, we conclude that this effect contributes negligibly to the overall response. Changes in the resulting S−S spacing of the 3MPT layer after deposition of the metal monolayer, with a concomitant effect on the cross-linked siloxane terminus of 3MPT, might also contribute to the overall energetics of UPD for these systems. Complications introduced by kinetic effects do not allow the importance of this factor to be definitively ascertained for these three systems. However, the siloxane bond is remarkably variable and flexible, with known examples of siloxane bond angles ranging from ∼120° to 180° in various silicon-containing molecules[119−121] and in vitreous silica.[114−118] Thus, this factor is also expected to be relatively small.

With the 3MPT "step up" strain and siloxane lattice strain concluded to be small contributions to the thermodynamic difference between Tl and Pb UPD on 3MPT-modified Ag and bare Ag, the predominant thermodynamic effect of 3MPT on the loss of underpotential stabilization must be the difference in strength between the 3MPT−Ag and the 3MPT−UPD monolayer/Ag bonds. Assuming minimal kinetic complications and complete discharge of Tl^+ and Pb^{2+} upon reduction to form their respective monolayers, if 3MPT binds to the UPD monolayer/Ag surface as strongly as it does to the bare Ag surface, then the underpotential stabilization should remain the same, and the peak potential for UPD monolayer deposition should be the same at 3MPT-modified Ag electrodes as it is at bare Ag. As the energy required to break the 3MPT−Ag bond becomes increasingly larger than the energy gained by the rebinding of 3MPT to the UPD monolayer/Ag surface, the underpotential stabilization of the metal monolayer will decrease, and the UPD peak will shift closer to the bulk metal deposition wave. For deposition of the first Tl monolayer, the underpotential stabilization, measured as the difference in peak potential between the first UPD monolayer deposition wave and the bulk metal stripping wave (not shown), decreases from ∼270 mV at bare Ag to ∼90 mV at 3MPT-modified Ag. Thus,

(119) Tossel, J. A.; Gibbs, G. V. *Acta Cryst. A* **1978**, *34*, 463−472.
(120) Baney, R. H.; Itoh, M.; Sakakibara, A.; Suzuki, T. *Chem. Rev.* **1995**, *95*, 1409−1430.
(121) Murugavel, R.; Voigt, A.; Walawalkar, M. G.; Roesky, H. W. *Chem. Rev.* **1996**, *96*, 2205−2236.
(122) Natan, M. *Inorg. Chem.* **1997**, *36*, 622−628.

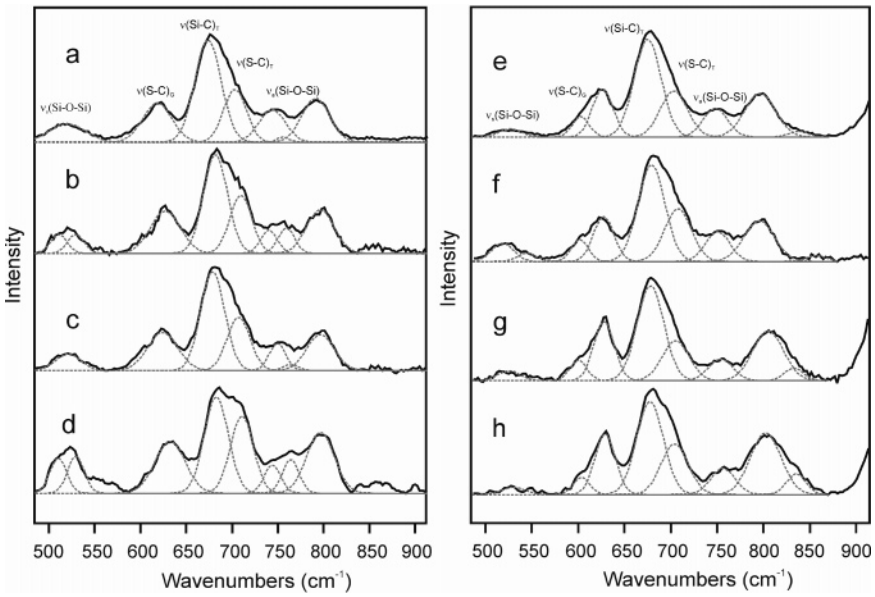

Figure 6. Surface Raman spectra acquired from emersed 3MPT-modified Ag electrodes in aqueous Tl^+ (1 mM Tl_2SO_4/0.1 M K_2SO_4/2 mM H_2SO_4) or Pb^{2+} (1 mM $Pb(NO_3)_2$/0.1 M $NaClO_4$/2 mM $HClO_4$) solutions: (a,e) at −200 mV prior to metal deposition, during the UPD of (b) Tl (−600 mV, ∼0.25 ML) and (f) Pb (−380 mV, ∼0.8 ML), (c,g) after returning the potential to −200 mV after the spectra were acquired in panels b and f, and the during bulk deposition of (d) Tl (−800 mV) and (h) Pb (−580 mV).

the 3MPT−Ag bond is ∼17 kJ/mol stronger than the 3MPT−Tl/Ag bond. For deposition of the first Pb monolayer, the underpotential stabilization decreases from ∼190 mV at bare Ag to ∼80 mV in the presence of 3MPT, indicating that the 3MPT−Ag bond is only ∼21 kJ/mol stronger than the 3MPT−Pb/Ag bond when accounting for the reduction of Pb^{2+} by two electrons. Given that the 3MPT−Ag bond must be broken in each case in order for UPD monolayer deposition, not as much energy is gained back by reforming the 3MPT−Pb/Ag bond as is gained by forming the 3MPT−Tl/Ag bond. Thus, the bonding of 3MPT at the Tl/Ag surface is concluded to be slightly stronger than the bonding of 3MPT at the Pb/Ag surface by ∼4 kJ/mol, although 3MPT binding at both monolayer-covered surfaces is considerably weaker than that at bare Ag.

Further evidence for the model shown in Figure 4 comes from vibrational spectroscopy on the Tl and Pb systems before, during, and after metal deposition. The results from these studies verify the stability of the 3MPT layer toward both underpotential and overpotential deposition of Tl and Pb. Figure 6 shows Raman spectra acquired in an emersion configuration[102−105] from both systems. In emersion, the 3MPT-modified Ag electrode rotates slowly through a drop of solution held to it by a small-bore capillary. Potential control is achieved in a three-electrode configuration using a Pt counter electrode inserted into the reservoir for the capillary and a AgQRE wrapped around the exterior of the capillary and inserted into the solution drop between the capillary and the electrode surface. As the sample rotates, a thin layer of solution (typically <5 nm[102]) is sheared from the bulk solution and can be sampled by Raman spectroscopy.[103−105]

Figure 6a,e shows the surface Raman spectra in the frequency region between 500 and 900 cm^{-1} for a hydrolyzed and condensed monolayer of 3MPT on Ag at −200 mV, prior to the onset of either Tl or Pb UPD, in aqueous solutions of the corresponding metal cations. This region contains vibrations associated with S−C, C−Si, and Si−O−Si bonds.[22,23] These spectra are similar to those previously reported from this laboratory for hydrolyzed and cross-linked 3MPT layers on Ag.[22,23,40] Previous studies have demonstrated that, upon hydrolysis and cross-linking, the monolayer takes on a relatively ordered structure, with the S−C bonds largely parallel to the surface and the C−Si bonds largely perpendicular to the surface.[22,23,40] Vibrational bands have previously been assigned as follows:[22,23] 524 cm^{-1} is the ν_s-(Si−O−Si), 627 cm^{-1} is the $\nu(C-S)_G$, 684 cm^{-1} is the ν(Si−C), 702 cm^{-1} (shoulder) is the $\nu(C-S)_T$, and 801 cm^{-1} is the ν_a-(Si−O−Si).

Raman spectra acquired upon deposition of partial monolayers of Tl (Figure 6b) and Pb (Figure 6f) are shown, as are spectra acquired after these when the potential was returned to −200 mV. Finally, panels d and h of Figure 6 show Raman spectra acquired during the deposition of bulk Tl and Pb, respectively. Although minor changes are observed in the peak positions of vibrations associated with the S−C and Si−O−Si bonds upon either UPD or bulk deposition of these two metals, overall, the spectra are relatively unchanged by the deposition of the foreign metal overlayer. Of greatest importance is that the spectral intensity of the 3MPT layer does not decrease upon UPD of either Tl or Pb. This observation supports the picture shown in Figure 4 that indicates no change in surface coverage of the electrode by 3MPT upon UPD. Moreover, the retention of spectral intensity for 3MPT, even during bulk metal deposition, in both cases supports the proposition stated above that the thiolate S atoms of the 3MPT layer rebond to the metal overlayer once it is deposited onto the Ag surface. Unfortunately, for the weak surface-enhancing Ag electrodes used for this study,[123] the ν-(metal−S) mode that would be expected in the region between 150 and 300 cm^{-1} is too weak to be observed on the Rayleigh scattering background associated with the single monochromator used for these studies.

Stability of 3MPT Layers to Repeated UPD of Tl and Pb. The above Raman spectral studies support the robustness of the hydrolyzed and cross-linked 3MPT layer toward metal deposition and stripping. The stability of the 3MPT layer to repeated metal deposition and stripping cycles was also assessed electrochemically, and the response compared to that of BT-modified Ag. BT was chosen for this comparison on the basis of its similarity in thickness to the 3MPT layer.

(123) Taylor, C. E.; Pemberton, J. E.; Goodman, G. G.; Schoenfisch, M. H. *Appl. Spectrosc.* **1999**, *53*, 1212−1221.

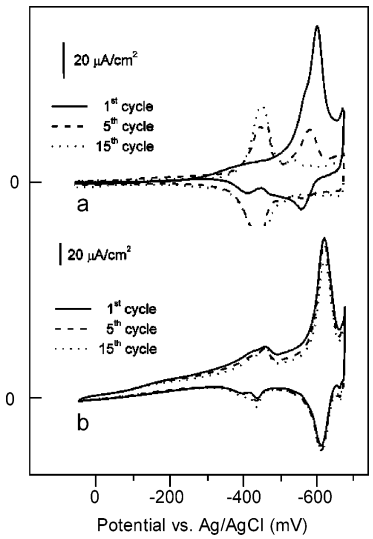

Figure 7. (a) Voltammetry for the 1st (solid line), 5th (dashed line), and 15th (dotted line) potential cycle for Tl UPD in 1 mM Tl_2SO_4/0.1 M K_2SO_4/2 mM H_2SO_4 at a BT-modified Ag surface; potential sweep rate of 25 mV/s. (b) Voltammetry for the 1st (solid line), 5th (dashed line), and 15th (dotted line) potential cycle for Tl UPD in 1 mM Tl_2SO_4/0.1 M K_2SO_4/2 mM H_2SO_4 at a 3MPT-modified Ag surface; potential sweep rate of 25 mV/s.

Panels a and b of Figure 7 show the 1st, 5th, and 15th voltammograms for Tl UPD at BT-modified and 3MPT-modified Ag electrodes, respectively. In the first cycle on BT-modified electrodes, a peak for Tl monolayer deposition occurs at −515 mV; this peak is shifted to more negative potentials than those at bare Ag, similar to the behavior observed for 3MPT-modified Ag. However, the Tl stripping process in the first scan exhibits significant differences from that on 3MPT-modified Ag. Instead of a single peak for Tl stripping, three stripping peaks are observed that correspond to the removal of Tl from beneath the BT monolayer (−500 mV) and from bare Ag (−400 and −380 mV). Thus, Tl deposition leads to partial displacement of the BT monolayer from the Ag surface in the first potential cycle. This loss of the BT monolayer by Tl deposition and stripping is similar to the previously reported loss of a propanethiol monolayer by stripping of a Cu UPD layer.[66]

In the fifth cycle, the peak at −515 mV decreases significantly (by ∼30%) with concomitant growth of a new deposition peak at −410 mV. In the stripping portion of the fifth cycle, the peak at −515 mV is greatly diminished at the expense of the peak at −390 mV, which represents a combination of the stripping peaks at −400 and −380 mV seen in the first cycle. In the 15th cycle, the peak at −515 mV has almost completely disappeared, while the peak at −410 mV has increased to a level corresponding to a majority (∼94%) of the Ag surface area. On the basis of these voltammetric responses, one concludes that repeated Tl monolayer deposition and stripping removes BT from the Ag surface.

In comparison to the limited stability of BT-modified Ag to repeated Tl deposition and stripping cycles, the stability of 3MPT-modified Ag is shown in Figure 7b. A cursory examination of these voltammograms leads to the immediate conclusion that 3MPT films are considerably more stable toward Tl deposition and stripping than are BT films. In the first cycle, ∼5% of the Tl monolayer is deposited at −475 mV corresponding to Tl deposition on bare Ag at defect sites. The remainder of the Tl monolayer is deposited in a single peak at −628 mV. This voltammogram is similar to that shown in Figure 1b with the exception that the two discrete Tl deposition peaks observed at 10 mV/s broaden into a single wave at −628 mV at 25 mV/s. Tl is stripped from beneath the 3MPT by a single broad peak at −609 mV.

In the fifth cycle, the peak at −415 mV for Tl deposition at defects in the 3MPT film increases slightly with a corresponding small decrease in the peak at −600 mV for Tl deposition at 3MPT-modified Ag. The voltammogram for the 15th cycle exhibits no significant changes from that for the 5th cycle, indicating that the majority of the 3MPT layer remains at the Ag surface. Thus, the stability of the 3MPT monolayer is strikingly better than that of the BT layer.

Additional insight into the thermodynamics of Tl UPD at BT-modified Ag compared to 3MPT-modified Ag can also be extracted from the voltammetry of these systems. Using the separation in peak potentials between the waves for deposition of the first Tl monolayer and bulk Tl (not shown) as an estimate of the magnitude of the underpotential at the BT-modified surface, a value of ∼190 mV is determined, slightly more than twice as large as the underpotential at the 3MPT-modified electrode. Thus, the Tl monolayer is *less* energetically advantaged beneath the 3MPT monolayer than beneath the BT layer by ∼100 mV or 9.6 kJ/mol. We postulate that, since the 3MPT layer is polymerized at its outer edge, the molecules cannot reorient upon Tl deposition to attain the optimized angles for the Ag−Tl−S−C bonding arrangement. Additional strain may also be conferred on the 3MPT monolayer by changes in the S−S spacing as the uppermost metal layer to which the 3MPT is bonded changes from Ag, with a radius of 0.144 nm, to Tl, with a radius of 0.171 nm.[111] Similar constraints do not exist for the BT monolayer, since all film molecules are structurally independent.

The stability of the 3MPT layer to repeated Pb deposition and stripping cycles was also investigated and compared to the stability of a BT layer subjected to the same treatment. The voltammograms from these systems are included in the Supporting Information and are essentially similar to those observed with Tl. However, the number of deposition/stripping cycles required to remove a given amount of BT from the surface by UPD Pb appears to be greater than that required by UPD Tl. For Pb UPD, the peak associated with Pb deposition on regions of BT-modified Ag decreases by only ∼2% over the first five cycles. In contrast, after five cycles of Tl deposition and stripping, ∼30% of the BT monolayer is removed. The magnitude of the underpotential for Pb monolayer deposition at BT-modified Ag is ∼70 mV compared to an underpotential of ∼190 mV for Pb deposition at bare Ag. In contrast, the magnitude of the underpotential for Tl monolayer deposition at bare Ag is ∼270 mV but only decreases to ∼190 mV at BT-modified Ag. The magnitudes of these underpotentials indicate that the Tl−Ag bond is weakened less by the BT layer by about the same amount as the Pb−Ag bond. Thus, the strength of BT bonding at the Pb-covered Ag surface must be comparable to the strength of BT bonding at the Tl-covered Ag surface. Hence, the greater BT desorption by Tl deposition compared to Pb deposition is somewhat surprising but may be due to the strength of desorbed butanethiolate binding to Pb^{2+} compared to Tl^+ in solution.

The stability of the 3MPT monolayer to repeated Tl and Pb UPD deposition and stripping cycles must be a consequence of the two-dimensionally polymerized siloxane terminus that prohibits loss of the film from the Ag substrate surface even when the Ag−thiol bonding is disrupted. The observation that the peak potentials for the UPD deposition process do not change in subsequent cycles indicates that the Ag−thiol bond is reformed after the loss of the UPD metal by anodic stripping. This observation suggests a potential use of such two-dimensionally polymerized 3MPT layers on metals to systematically alter the

chemical nature or electrochemical stability of the surface by foreign metal UPD in a robust reproducible manner.

Conclusions

3MPT monolayers are shown to provide exceptionally stable SAMs due to cross-linking of the ω-terminus while still providing reactive, functional surfaces for additional layer fabrication. These UPD studies provide a more detailed molecular understanding of interfacial structure. Tl and Pb are both shown to undergo UPD at Ag surfaces modified by two-dimensionally cross-linked layers of 3MPT. The absence of a well-defined UPD wave for Cd strongly supports our proposed mechanism for Tl and Pb UPD involving the penetration of hydrated Tl^+ and Pb^{2+} through the 3MPT structure via openings in six-membered siloxane rings at the 3MPT−solution interface. This postulated mechanism for UPD through the 3MPT monolayer is consistent with the Stokes diameters of these cations.

For Tl and Pb UPD, the presence of the 3MPT monolayer decreases the thermodynamic advantage for UPD relative to bare Ag surfaces by an amount corresponding to the difference in energy between the 3MPT−Ag and 3MPT−Tl/Ag or 3MPT−Ag and 3MPT−Pb/Ag bonds. These decreases in bond energies result in shifts of the UPD monolayer deposition waves to more negative potentials. Minor kinetic inhibition of mass transport, which is also a function of cation Stokes diameters, is also observed for these underpotential metal deposition processes, as manifested by an increase in the peak potential separation of the monolayer deposition and stripping waves.

Acknowledgment. The authors gratefully acknowledge support for this research from the National Science Foundation (CHE-0317114) and the Department of Energy, Office of Basic Energy Science (DE-FG03-95ER14546). The authors also thank Dr. Anoma Mudalige for technical assistance.

Supporting Information Available: Voltammetry for the first 60 potential cycles for Pb UPD in 1 mM $Pb(NO_3)_2$/0.1 M $NaClO_4$/2 mM $HClO_4$ at a BT-modified Ag surface, and voltammetry for the 1st, 5th, and 45th potential cycles at a 3MPT-modified Ag surface. This material is available free of charge via the Internet at http://pubs.acs.org.

LA063137X